Available online at www.sciencedirect.com
ScienceDirect
International Journal of Mass Spectrometry 258 (2006) 104–112
International Journal of Mass Spectrometry
www.elsevier.com/locate/ijms

Component and morphology biases on quantifying the composition of nanoparticles using single-particle mass spectrometry

L. Zhou, A. Rai, M.R. Zachariah *

Department of Mechanical Engineering and Department of Chemistry and Biochemistry University of Maryland, College Park 20742, USA

Received 28 April 2006; received in revised form 7 July 2006; accepted 11 July 2006
Available online 28 August 2006

Abstract

Considerable effort has been expended to develop the real-time single-particle mass spectrometry using the laser ablation/ionization technique. With a complete ionization technique, quantitative information about particle size and elemental stoichiometry for a single component particle can be obtained. However, it is more complex to deal with multi-component composite particles. The morphology and the composition of particles will change the thermal and optical properties of the particle and thus the laser-particle interaction. In this paper, multi-component particles of different morphologies are generated and used to examine the limitations of the complete ionization approach. The experimental results show that there are component and morphology biases, which can be related to the high non-linear properties of the laser-particle interaction. The relative laser absorbtivity of each component is found to have a significant impact on the particle heating and ion formation process. In addition, the ion distribution formed from the laser-particle interaction is in part a result of charge transfer, and electron-ion recombination. A qualitative explanation for the observed behavior is developed, which involves the characteristic time for laser heating and intraparticle heat conduction.

Keywords: Single-particle mass spectrometry; Nanoparticle; Morphology and component bias

1. Introduction

Single-particle mass spectrometry has been widely studied and used in the past decade as a tool for real-time elemental characterization of individual particles [1–8]. In this method, an aerosol sample is continuously introduced into the ion source region of a mass spectrometer using a high throughput source, such as an aerodynamic lens system. Subsequent, laser ablation/ionization and time-of-flight (TOF) analysis are used to obtain single-particle mass spectra. The ultimate goal of this method is to quantitatively characterize the size, elemental composition and gas-particle reactivity of aerosols [1,3,4,9].

In principle, the mass spectrum should provide quantitative information about the particle composition and size, however, due to the complexity of the transport and ion-generation/detection, quantitative interpretation is normally not achieved. In their study of the oxidation state of chromium in aerosol particles, Neaubauer et al. showed that the distribution of ions in the corresponding mass spectra is influenced by many factors including particle size, composition, laser irradiance, wavelength and mass spectrometer operating conditions [10]. Moreover, the study of atmospheric aerosols by Zelenyuk and Imre suggests that there are significant limitations in laser ablation technique, namely the highly non-linear nature of the ablation process, which makes quantitative calibration of mass spectra extremely difficult to realize [1]. They also suggested that the mass spectrum was dominated with the low ionization potential species. Reilly et al. have studied the charge-transfer-induced matrix effects in the laser ablation process for micron-sized environmental aerosols [11]. Their results suggest that for multi-component particles, the species with low ionization potential is easily detected in most matrices and species with high ionization potential may only be detected in matrices with higher ionization potential. Ge et al. have used single-particle mass spectrometry to study micron-sized multi-component particles with different chemical morphology. Their results show that particles were partially vaporized/ionized during the ion formation process, so that only the surface layer of the particle can be explored [12]. They further studied the size and composition biases for ultrafine particles [13,14], and showed that the ion

* Corresponding author.
E-mail address: mrz@umd.edu (M.R. Zachariah).

1387-3806/$ – see front matter © 2006 Elsevier B.V. All rights reserved.
doi:10.1016/j.ijms.2006.07.006

Table 1
Summary of particle morphology and component properties

Particle component	Particle morphology	Component properties	
		Core	Shell
Sodium chloride[a]	Single component	N.A.	N.A.
Aluminum/sodium chloride[b]	Core–shell	Absorbing (Al)	Transparent (NaCl)
Aluminum oxide/sodium chloride[c]	Core–shell	Transparent (Al_2O_3)	Transparent (NaCl)
Aluminum oxide/sodium chloride[d]	Matrix	N.A.	N.A.
Aluminum oxide/nickel[e]	Core–shell	Transparent (Al_2O_3)	Absorbing (Ni)
Aluminum/carbon[f]	Core–shell	Absorbing (Al)	Absorbing (C)

[a] Fig. 3.
[b] Fig. 4.
[c] Fig. 5.
[d] Fig. 6.
[e] Fig. 8.
[f] Fig. 9.

yields vary with different species, and the detection efficiency is a strong function of size and composition of nanoparticle due to the inlet transmission characteristics and the intrinsic nature of the laser-particle interaction.

These results suggest that the detection sensitivity is strongly biased with species and the spectrometer operating condition. Thus, to achieve the goal of quantitative characterization of individual aerosol particles using single-particle mass spectrometry, it becomes imperative that we understand the sensitivity biases in the spectrum. Efforts to overcome the limitation of laser ablation/ionization mass spectrometry, include a two-laser approach used by several researchers to optimize the vaporization and ionization steps [15–17]. In another approach Reents et al. used a highly focused laser to create an extremely hot plasma, such that all elements are converted to positive ions even for electronegative species. This approach has been used by other research groups as well. Wang et al. recently developed a nanoaerosol mass spectrometer (NAMS) that uses this complete ionization technique. Quantitative chemical characterization for particle with diameter ∼10 nm was achieved with a quadrupole ion guide and quadrupole ion trap system [18]. A similar technique of using a very high fluency laser (>10^{11} W/m^2) beam has also been employed in our group, and in our previous studies quantification of composition and size for various nanoparticles have been achieved with reasonable accuracy [4,19].

In this paper, we report recent findings which show that although this complete ionization technique can accurately characterize single component particles, the situation becomes more complex when one is dealing with multi-component particles whose composition is not homogeneous within the particle. Essentially, we want to explore the relationship between how the elemental components are mixed within a particle, and the resulting mass spectrum. The study is conducted by generating coated and composite particles, and correlating the results to the relative absorbtivity of the coating material relative to the core. To explore and explain these effects, several different types of composite particles were studied in this work: (i) aluminum particles coated with sodium chloride, (ii) aluminum oxide particles coated with sodium chloride, (iii) aluminum oxide and sodium chloride matrix particles and (iv) aluminum oxide particles coated with nickel. A summary of the morphology and component properties of testing particles are shown in Table 1. We show that the nature by which the constituents of the particle are assembled, and the relative absorptivity of the constituent materials to the laser, has a profound influence on the resulting mass spectrum. The mass spectra of these particles were evaluated to understand the component/morphology biases of the spectrometer. To our knowledge, the work reported here is the first finding on the composition/morphology biases for single-particle mass spectrometer (SPMS) using the complete laser ionization technique. We also develop a qualitative explanation for the observed behavior.

2. Experimental

2.1. Single-particle mass spectrometer

The single-particle mass spectrometer used in this study consists of an aerodynamic lens inlet, a three-stage differential pumping system, a free-firing dissociation/ionization laser and optics system, a linear time-of-flight (TOF) tube with a cylindrical Einzel lens and data acquisition system, as shown in Fig. 1. Detailed descriptions on the SPMS can be found in our previous papers [4,19]. Briefly, the aerodynamic lens inlet is employed to produce a narrow collimated beam of particles that can be injected with high transport efficiency through differentially pumped chambers to the ionization region. The pressure in the ionization chamber which houses the time of flight tube is $\sim 6 \times 10^{-7}$ Torr when the aerosol inlet is open. The laser used in this system is a frequency-doubled Nd:YAG operated at 10 Hz in the internal Q-switch mode. The laser energy measured before the laser entrance window of the mass spectrometer was ∼100 mJ/pulse, was focused with an in-chamber mounted 38 mm focal length focusing lens, to give a ∼0.3 mm diameter beam. The laser power density of the 5 ns pulse at the focal point, is estimated to be approximately ∼10^{11} W/cm^2. Positive ions formed during ionization of particle are accelerated along ∼1 m long linear TOF tube, and are detected by a microchannel plate (MCP) detector.

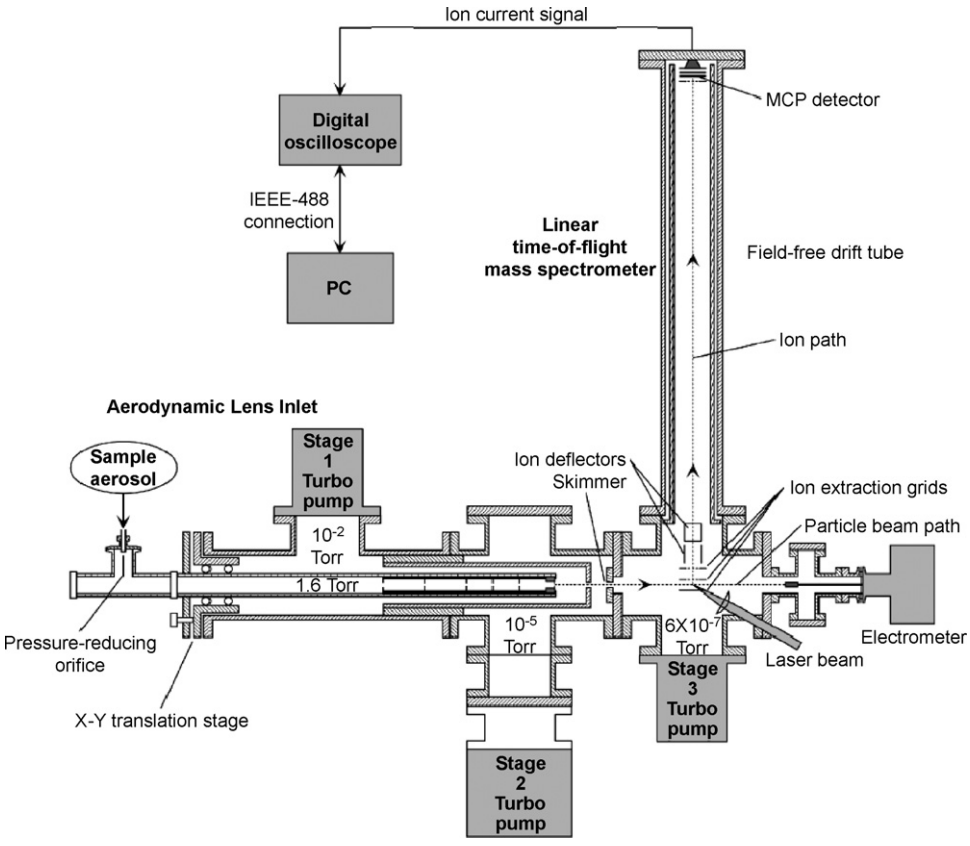

Fig. 1. Schematic of single-particle mass spectrometer (SPMS).

2.2. Generation of test nanoparticles

The schematic of the experimental setup used to generated test particles is shown in Fig. 2. Polydisperse droplets were produced from an atomizer that contained a solution or suspension of known composition. Aerosol dryers filled with dry silica gel were used to control the water content of the test particles coming out of the atomizer. Subsequently, the particle stream was passed though a heated flow tube with a heated length of 30 cm, and then delivered to the SPMS inlet.

This system was used to generate multi-component particles with different morphologies. Commercially available aluminum nanopowder from Aveka Inc. with primary particle size of 50 nm was mixed with NaCl and was dispersed in 100 mL DI water and atomized. After the removal of the solvent (water) by diffusion drying, salt-coated aluminum resulted as verified by TEM. Aluminum oxide coated with NaCl was obtained in a similar way by dispersing aluminum oxide and NaCl in DI water. The aluminum oxide was first generated by spray pyrolysis of aluminum nitrate aerosols in the tube furnace at a temperature of 500 °C, and collected on a Millipore filter. Nanoparticles containing a matrix of Al_2O_3/NaCl were formed using an approach presented in our previous work [20]. A solution of aluminum nitrate and NaCl in DI water was atomized and passed through a tube furnace at 500 °C to decompose the aluminum nitrate to aluminum oxide. This resulted in the formation of a matrix of Al_2O_3/NaCl particle. To obtain aluminum oxide particles coated with nickel, aluminum oxide and nickel nitrate were dispersed in a solvent of 30% ethanol and 70% DI water and were aerosolized. This aerosol stream was then heated to a temperature of 900 °C in a tube furnace. At this temperature, nickel nitrate decomposes to nickel metal, and forms a coating on the aluminum oxide particles [21].

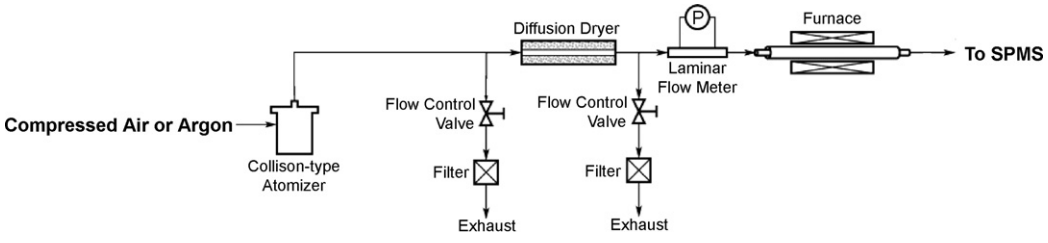

Fig. 2. Schematic of the particle generation system.

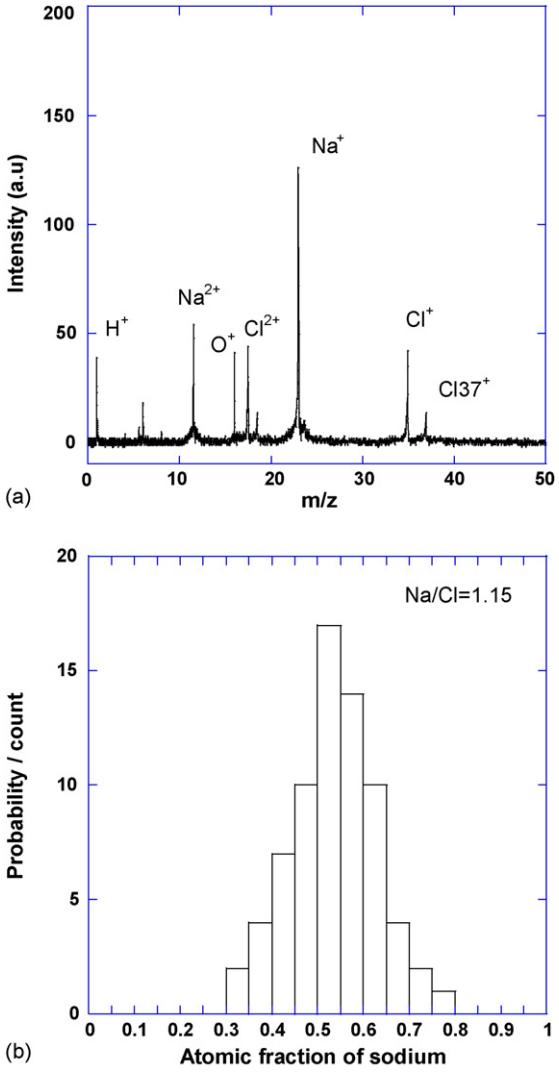

Fig. 3. (a) Typical mass spectrum of pure NaCl particles and (b) probability distribution of measured stoichiometry ratios for 70 NaCl particles.

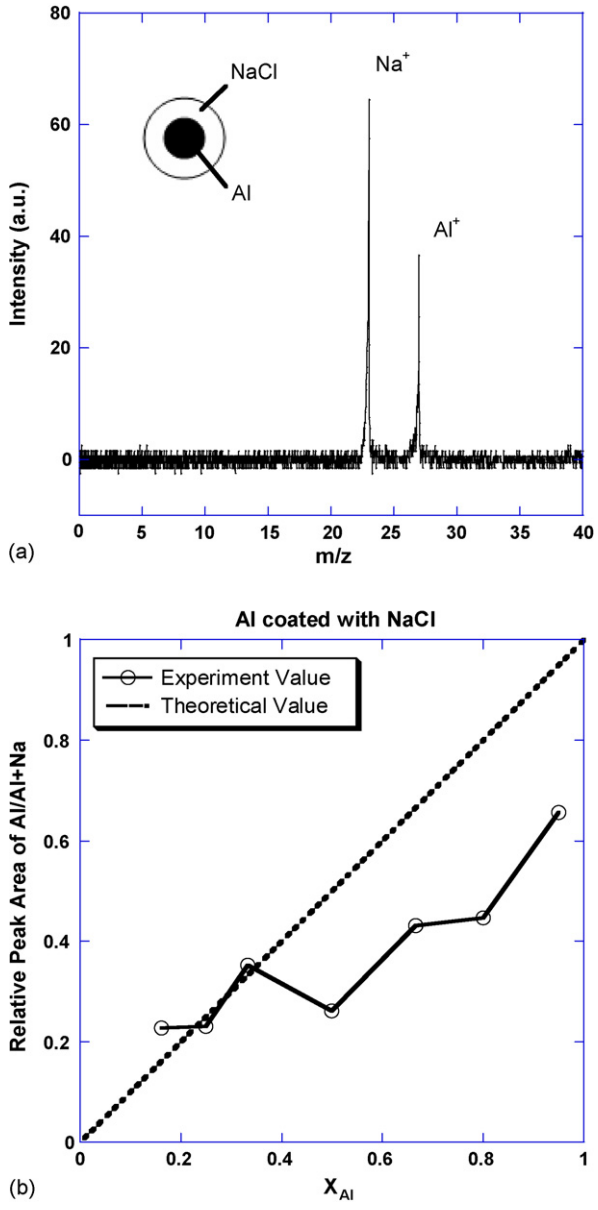

Fig. 4. (a) Typical mass spectrum of aluminum coated with NaCl (aluminum elemental mole fraction of $X_{Al} = 0.95$) and (b) relative aluminum elemental mole fraction for aluminum particles coated with NaCl.

3. Results and discussion

In our prior work [4,19], we employed a highly focused laser beam, which enabled us to achieve high ionization for all elements in a single particle, enabling us to determine the elemental stoichiometry to within 15%. An example of a typical mass spectrum for a single sodium chloride particle is shown in Fig. 3(a). Fig. 3(b) presents the resulting probability distribution of measured stoichiometric ratios for 70 NaCl Particles. Considering the very large difference in the ionization potentials of Na and Cl, the results are an indication of the robustness of the quantitative nature of the total ionization method.

However, these results beg the question as to whether it matters how the components are arranged within the particle. The most obvious controllable morphology is a coated particle. We begin with Al/Al_2O_3 particles coated with NaCl. An example of a typical mass spectrum for aluminum particle coated with NaCl is shown in Fig. 4(a). The spectrum shown in the figure is for a coated particle which was obtained by aerosolizing a mixture of aluminum and sodium chloride such that the mole ratio of aluminum, $X_{Al} = 0.95 (X_{Al} = m_{Al}/(m_{Al} + m_{NaCl}))$. A point of note is that the mass spectrum shows an abnormal behavior with strong peaks for Al and Na, but the absence of any chlorine peak. This is unlike the spectrum of pure salt particle (Fig. 3(a)), in which chlorine cations can be easily observed. This particular particle consists of a relatively large aluminum core with a small salt coating, however, the sodium ion intensity is larger than the more abundant aluminum. Fig. 4(b) shows the variation of elemental composition as the mole fraction of aluminum is varied in the suspension. The relative peak areas of Al/Al + Na are plotted versus relative mole concentration of elemental aluminum X_{Al} in the suspension. Each data point is an average of 100 single-particle mass spectrums. An ideal relationship should be a straight line with slope of 1 passing through the origin. What we

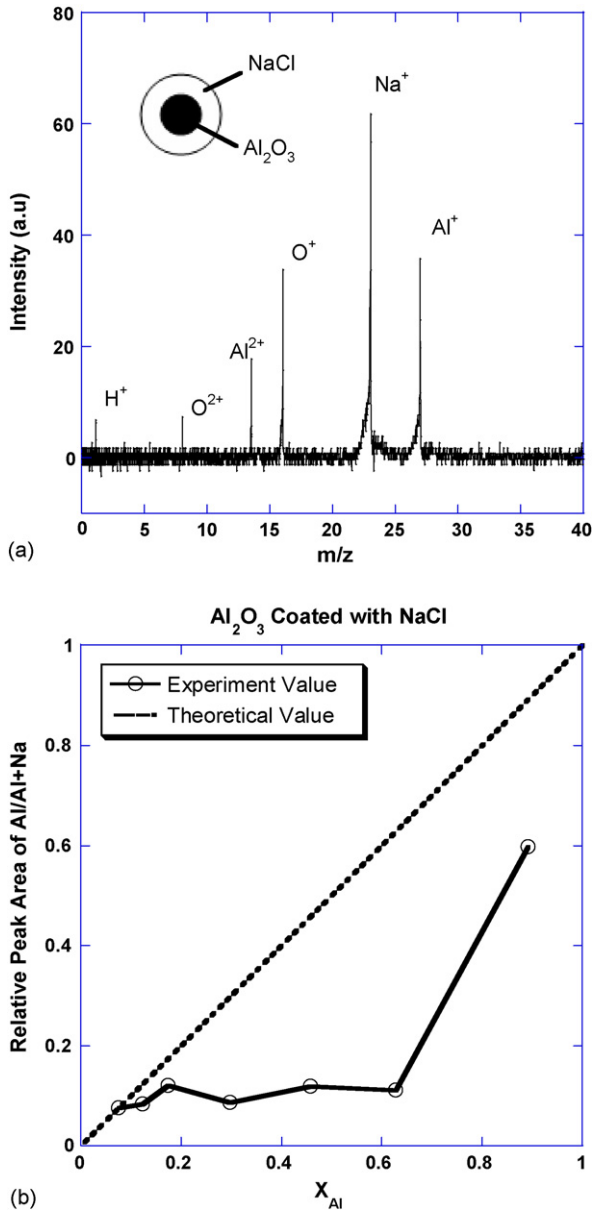

Fig. 5. (a) Typical mass spectrum of aluminum oxide coated with NaCl with aluminum elemental mole fraction of $X_{Al} = 0.90$ and (b) relative aluminum elemental mole fraction measurements for aluminum oxide particles coated with NaCl.

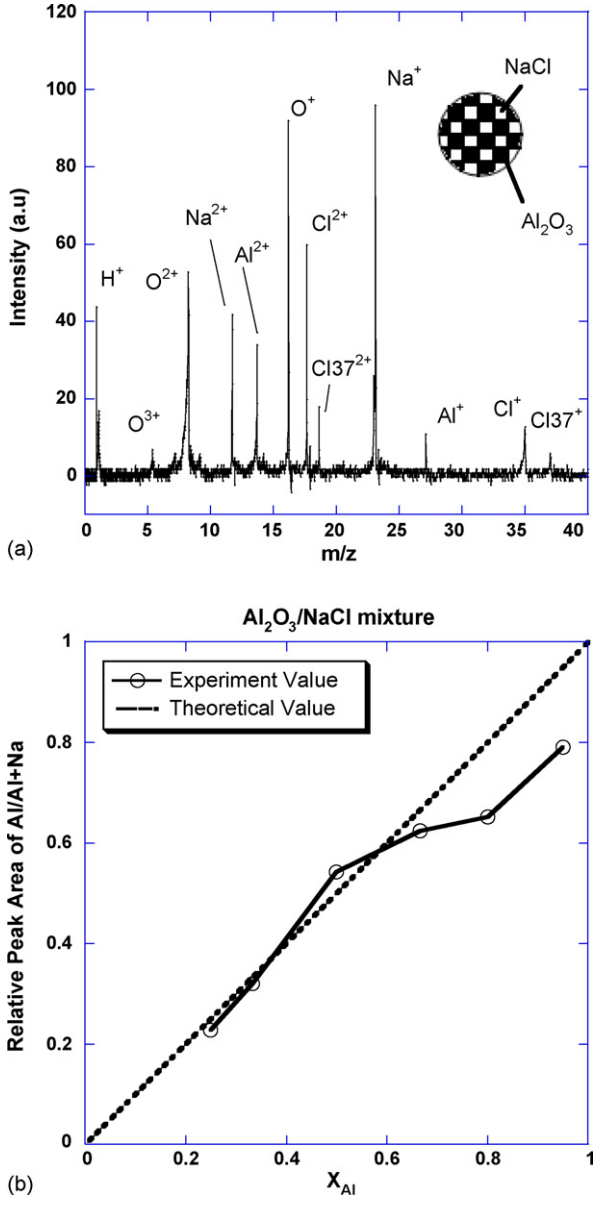

Fig. 6. (a) Typical mass spectrum for aluminum oxide and NaCl matrix particle with aluminum elemental mole fraction of $X_{Al} = 0.25$ and (b) relative aluminum elemental mole fraction measurements for aluminum oxide and NaCl matrix particles.

observe, however, is that the Al/(Na + Al) ratio is much lower than the theoretical value at all mole fractions of aluminum. Additionally, no Cl signal was seen in any spectra, even at high salt concentration.

Similar experiments were repeated for aluminum oxide particles coated with NaCl. The mass spectrum collected for aluminum oxide particles coated with NaCl also shows a similar behavior. Fig. 5(a) shows a typical spectrum for an aluminum oxide nanoparticle coated with sodium chloride. This spectrum was collected for a particle, which was formed by aerosolizing a suspension with mole fraction of elemental aluminum, $X_{Al} = 0.90 (X_{Al} = 2m_{Al_2O_3}/(2m_{Al_2O_3} + m_{NaCl}))$. An important point to note from this figure is that although we do observe multiply charged ions of aluminum ($m/z = 13.5$) and oxygen ($m/z = 8$), which would seem to indicate roust plasma formation, no chlorine peak was observed. The small N peak ($m/z = 14$) comes from the uncompleted decomposition of aluminum nitrate, which was used to form the aluminum oxide particles. We also looked at the variation of elemental composition as measured by the SPMS by varying the elemental aluminum mole fraction, and these results are plotted in Fig. 5(b). It can be seen that in this case as well, we are overestimating the sodium content in the multi-component particle, similar to the previous case of aluminum coated with NaCl.

However, a quite different result is obtained if homogeneous particles of the components are prepared. Fig. 6(a) shows a spectrum obtained at $X_{Al} = 0.25$, which clearly shows that all the elements including Cl are observed in the spectrum, and multi-

ple charged ion peaks suggest very aggressive plasma formation, and laser-particle interaction. There does, however, seem to be a bias against Cl cation formation at high mole fraction of Al. A plot of the variation of relative elemental composition with change in elemental aluminum mole fraction is shown in Fig. 6(b). The plot shows that the measurement of the Al/Na ratio is considerably improved over that seen for the salt-coated aluminum oxide (see Fig. 5b). In this plot, we can see that the measured elemental ratio for aluminum and sodium matches closely to the theoretical value at all mole fractions of aluminum. However, unlike the pure salt case, the Na/Cl ratio is much larger than unity. Although, we see chlorine in the spectrum, it is relatively weak as compared to the signals from other species.

As mentioned previously, we can determine the relative elemental concentration to within 15% for single-component particles [4]. However, for particles with the core–shell structure, the measured composition shows considerable error. In the core–shell structure discussed above, Na is higher than the theoretical value, so that the measured mol ratio of Al/Al + Na is lower than the true value. On the other hand, for homogeneously mixed Al_2O_3/NaCl particles, we observe that the results show relatively good agreement.

Our next task then is to attempt to resolve these observations. A particle undergoes three processes after it is delivered into the SPMS inlet: initially the particle is transmitted to the ion source region through an aerodynamic lens inlet. Subsequently in the ion source region, the particle is ionized by the focused laser beam. Finally, these ions are extracted by an electrical field and are transported through the TOF region, and reach the detector. Kane and Johnston showed that the particle transmission efficiency through the aerodynamic lens is biased by particle shape and size [13]. However, it is reasonable to assume that transport biases would not be significant for a homogeneous versus a core–shell structure, nor would they cause the errors in the measurement of elemental ratio for those particles that are ablated/ionized.

The other two possibilities are: (i) the ion formation/recombination process for these multi-component particles is component/morphology biased even at such high laser fluences. (ii) Ions are lost during transport in the TOF region of the mass spectrometer, and some species are selectively lost (e.g., ions with very high energy).

In our previous work, we evaluated ions transport losses in the TOF tube, and a model was developed to describe the preferential loss of the high kinetic energy ions [19]. This work indicated that one could, through the use of an Einzel lens system significantly increase the transmission (detection) efficiency of high kinetic energy ions. To explore this as a possible explanation of our observation we repeated the experiments with an Einzel lens voltage varied from 0 to 4000 V. One such result is shown in Fig. 7, for the salt-coated aluminum oxide particles. While the use of the lens did change ion intensity, indicating that we could use the lens to transport more ions down the flight tube, Fig. 7 clearly shows that the lens has no effect on the relative ion signal. This result would seem to indicate fairly convincingly that whatever the ion energy distribution might be, that all species would seem to have a similar distribution as produced

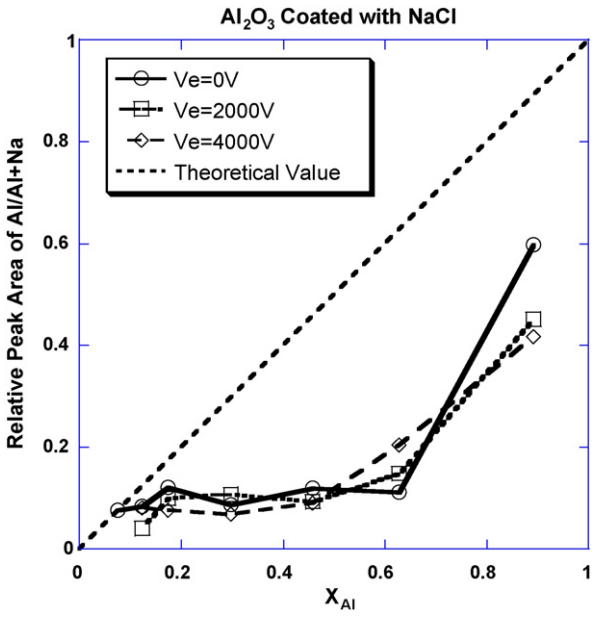

Fig. 7. Effect of Einzel lens on relative aluminum elemental mole fraction measurements for aluminum oxide particles coated with NaCl.

in the laser induced plasma, and we should expect no transport biases in the flight tube.

Based on the above observations, the most likely explanation of the experimental results would involve the interaction between particle and laser pulse. Considerable research has been directed to investigate the mechanism of the laser-particle interactions [22–24], which involves the process of energy absorption, particle heating, melting/evaporation and subsequent fragmentation/ionization of the particle. These highly non-linear processes are very complex, and are influenced by both the laser beam parameters, and the particle optical/thermal properties. Clearly particles with different morphology, and/or composition will have different optical/thermal properties, which may influence the interaction process, and thus the resulting ion distribution. In our previous work, we applied a hydrodynamic model [24,25] to explain the laser-particle interaction. For the laser intensity used in this study ($\sim 10^{11}$ W/cm^2), the particle is first heated by the laser beam, and subsequently ionized by a hydrodynamically controlled ionization process. The heating rate of the particle is given by

$$\text{heating rate} = \frac{1}{2}\omega Im(\gamma)|E|^2 \tag{1}$$

where ω is the laser frequency, E the electrical field generated by the laser beam and Im(γ) is the imaginary part of particle polarizability, which is given by

$$Im(\gamma) = \frac{6a^3nk}{|N|^4 + 4(n^2 - k^2) + 4} \tag{2}$$

where a is the particle radius and $N = n + ik$ is the complex refractive index of particle. For the laser frequency used in this work, aluminum has a complex refractive index of $N = 0.15 + 5.35i$, and aluminum oxide is $N = 1.77 + 10^{-6}i$ indicating that aluminum is a much stronger absorber than aluminum oxide. For NaCl, we

found that $N = 1.54 + 0i$, which indicates that NaCl is virtually transparent to the laser beam. When we have pure salt, presumably the threshold before heating and ionization takes place is much higher than that for pure aluminum. For aluminum particles coated with sodium chloride, the coating is, relative to the core transparent to the laser beam, and thus the laser beam should first interact with the core of the coated particles. This could cause local heating and subsequent plasma formation of the core, with energy conduction to the shell. In this case, our observed results are consistent with the idea that the heating from the core is sufficient to just blow the shell-off but not intense enough to cause significant ionization of the shell material as evidenced by the lack of signal for Cl. We will defer for the moment an explanation for why the Na signal is actually higher than expected relative to Al.

For aluminum oxide particles coated with NaCl, although we believe that aluminum oxide can absorb more laser energy during the laser-particle interaction as compared to NaCl, the above analysis is hard to validate because the imaginary part of the refractive index for Al_2O_3 is also small. Thus, it may take a longer time for the Al_2O_3 core to absorb sufficient energy to create a plasma. During this heating period, there is also thermal conduction between the Al_2O_3 core and the NaCl coating due to the temperature inhomogeneity between the two phases.

We begin with a comparison of the characteristic times for laser heating versus intra-particle conduction. The characteristic time for conduction, τ_s, can be estimated as:

$$\tau_s = \frac{a^2 \rho C_V}{\chi} \tag{3}$$

where χ is the thermal conductivity of the material, ρ the density of the material and C_V is the specific heat of the material.

In the hydrodynamic model [24,26], it was demonstrated that the laser energy absorption is enhanced near the critical density surface. The critical electron density is given by

$$N_{cr} = \frac{m\omega^2}{4\pi e^2} \tag{4}$$

Below this density, the plasma becomes transparent to the laser beam and does not absorb any further energy. In our previous work [25], we have shown that during the laser-particle interaction, the electron density profile in the plasma is non-uniform and one can find a critical density surface where resonant laser energy absorption occurs. The electric field is also significantly enhanced in the regions close to the critical density surface. The time to achieve the resonant laser absorption in the plasma can be defined as the critical density lifetime, τ_{cr} after which the plasma no longer absorbs energy from the laser. The critical density life time τ_{cr}, is given by [26]

$$\tau_{cr} = \frac{a}{c_s}\left(\frac{N_{e0}}{N_{cr}}\right)^{1/3} \tag{5}$$

where c_s is the plasma sound speed. For plasma temperatures of about 10 eV, c_s is estimated to be $\sim 3.6 \times 10^4$ m/s. N_{e0} is the initial electron density, $N_{cr} = m\omega^2/4\pi e^2$ is the critical density and (N_{e0}/N_{cr}) is of the order of 10.

For a 100 nm diameter particle, we calculate the characteristic times for the two processes. For aluminum oxide $\tau_s \sim 10^{-8}$ s and $\tau_{cr} \sim 10^{-12}$ s, and for aluminum they are $\tau_s \sim 10^{-11}$ s and $\tau_{cr} \sim 10^{-12}$ s. The comparison between the two time scales suggests that the energy absorption by the core is fast relative to thermal conduction, and particularly so for the aluminum oxide coated case. So, for aluminum oxide particles with a NaCl coating, the core will absorb energy and reach the critical point before it can conduct the energy to the shell. This is consistent with our thinking that having a transparent medium as the shell will result in poor coupling of the laser energy into the shell and a weak plasma formation. In other words, there exists a temperature gradient within the particle.

It is also interesting to note that at small X_{Al}, the composition of the particle is primarily NaCl with a small core of aluminum or aluminum oxide. So one would expect that the spectra obtained are similar to the spectra from pure salt particles. In fact the experimental observations imply that even a small change in the composition and structure of particles may influence the laser-particle interaction and may result in different ion distribution.

In contrast with the transparent coating, if the particle is coated with a light absorbing material, one would expect the laser to preferentially initially interact with the material on the shell. A significant difference for this morphology is that, even as the shell blows off as a dense plasma, the core can still be vaporized/ionized by the laser, although it might occur slightly delayed in time. As a consequence, the spectrum should show all the species present in the particle. Experiments were conducted to evaluate a more transparent material coated with a light absorbing material using aluminum oxide particles coated with nickel as a model system. Fig. 8(a) shows a typical spectrum obtained at mole fraction of aluminum, $X_{Al} = 0.90$, and it is clear that all the elements are detected in the spectrum in contrast to the salt-coated case. Fig. 8(b) shows the measured relative ratio of Ni to Al, and clearly show that the SPMS does a reasonable good job of measuring the elemental ratios. This is also consistent with our previous work [27], where we created a core–shell structure of carbon-coated aluminum. In this case, we have core–shell structure where both the core and the shell are highly absorbing. A typical mass spectrum obtained from experiment is plotted in Fig. 9, and it also shows that both the material on the core (aluminum) and shell (carbon and hydrogen) were observed. We were able to show in this prior work that we could, when compared with TEM, measure the thickness of the carbon coating.

We now turn our attention to multi-component matrix particles. The experimental observation suggests that the spectra obtained are also dependent on the relative concentration of each component. At high NaCl concentration, Cl can be detected. Also, although we can have a reasonable result for Al/Na ratio, the electro-negative specie Cl is still under-predicted in the spectra. This suggests that even for homogeneously mixed multi-component particles, there are composition biases for the laser ablation process. The possible reasons that may be responsible for these observations include charge transfer effects, and ion-electron recombination. Reilly et al.'s work showed that charge transfer in the laser ablation process has a significant influence

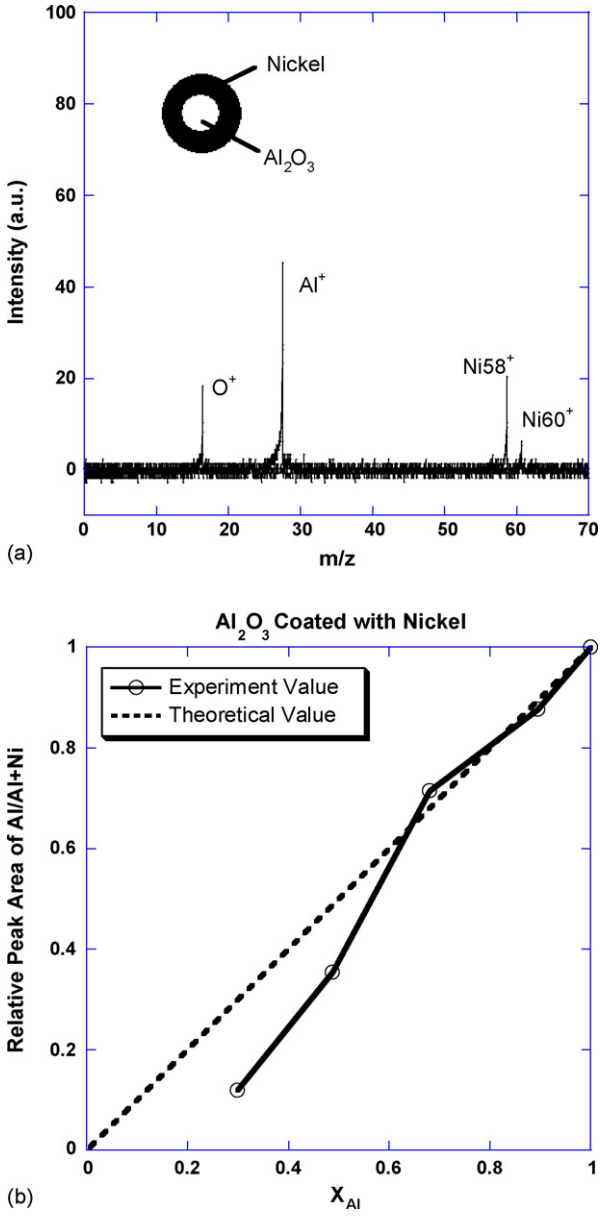

Fig. 8. (a) Typical mass spectrum for aluminum oxide coated with nickel with aluminum elemental mole fraction of $X_{Al} = 0.90$ and (b) relative aluminum elemental mole fraction measurements for aluminum oxide particles coated with nickel.

on the resulting ion distributions, and lowering the detectability limits for electro-negative cationic species relative to electro-positive species [11]. Since Cl has a high ionization potential (IP), and high electron affinity, the positively charged Cl ions are more likely to be neutralized by electron transfer from an electro-positive species or from free electrons. For a particle with low NaCl concentration, it may be possible that most of the Cl ions generated by the plasma are neutralized so that we do not detect any Cl signal in the spectra. However, for a particle with high NaCl concentration, the abundant Cl ions present in the plasma may cause saturation in the charge transfer, and ion-electron recombination process to form a Cl cations. To give a quantitatively explanation for the experimental observation, a complete understanding for the plasma formation/ion generation coupled

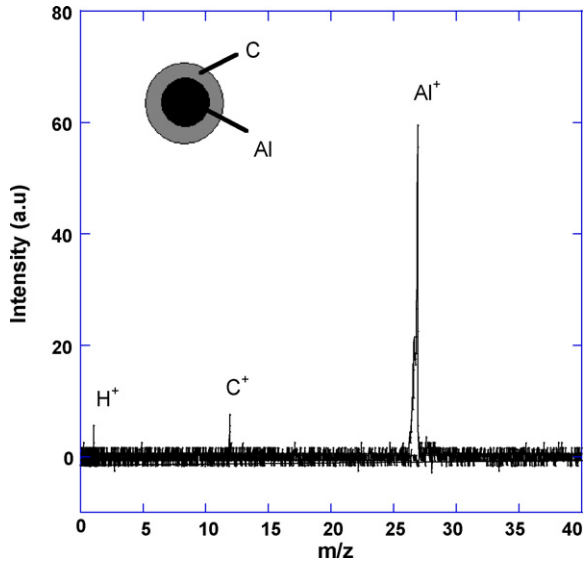

Fig. 9. Typical mass spectrum for aluminum particle coated with carbon.

with the charged transfer/ion-electron recombination process is required.

The above experimental results and analysis suggests that:

(a) The total ionization approach should work well for a homogeneous dispersed mixture of materials comprising a particle regardless of their relative absorptivity (e.g., Al_2O_3/NaCl matrix particle).
(b) The total ionization approach should work well for a core–shell structure if both components are strong absorbers or if the stronger absorber is the shell (e.g., carbon coated aluminum particle).
(c) The total ionization approach does not work well for a core–shell structure in which a weak absorber surrounds a strong absorber (e.g., NaCl coated aluminum or aluminum oxide particle).
(d) The total ionization approach does not work well for quantitatively characterizing the electric-negative species in a multi-material particle regardless of the morphology (e.g., Cl in Al_2O_3/NaCl matrix particle).

There is one additional point to consider in class (c) particles. Our experimental observations presented in Figs. 4(b) and 5(b) show that the core material was under-represented relative to the shell in terms of Na, even though it was the stronger absorber, and over -represented relative to the shell in terms of Cl. The only plausible explanation for this observation is charge transfer. It is quite reasonable to assume that for the case of aluminum coated with salt that as the salt is being blow-off, and since it was not ionized directly from the laser, that charge transfer between elements in the core and shell material should take place. In this case Na, which is easily ionized, and has a lower IP than Al, will donate an electron to Al, thereby neutralizing it, and decreasing the relative Al signal. On the other hand, chlorine has the highest IP, and a high electron affinity will, for the low temperature plasma shell, find itself certainly not forming cations, but possibly anions. Analysis of negative ions in the mass-spectrometer

showed only an electron signal implying that the negative ion signal is too small to be detected.

The above discussion gives a qualitative explanation for the experimental observations. However, to achieve the goal of quantitatively characterizing nanoparticles by using SPMS, a more detailed explanation is needed to understand the mechanism of laser-particle interactions.

4. Conclusions

In this article, we have reported our recent observations of morphology/component biases in characterization of multi-component particles using single-particle mass spectrometry. We studied core–shell and homogeneously mixed multi-component particles to understand the morphology biases in particle characterization using the complete ionization technique. We observed that for a core–shell structure, with a strongly absorbing material in the shell, the complete ionization technique gives a good elemental ratio for the electropositive elements. On the other hand for a weakly absorbing shell, errors in the elemental composition measurement correlate with the ionization potential of the elements. Homogeneously mixed matrix particles generally should give quantitative ratios for electropositive elements. However, we always observe that electronegative species are under-predicted for a multi-component particle. A qualitative explanation for the observed behavior was developed in this work, and we believe that this behavior is strongly associated with the particle thermal/optical properties, and the complicated nature of the laser-particle interaction process. The experiment results suggest that to overcome these limitations a detailed explanation of laser ablation/ionization process is needed.

References

[1] A. Zelenyuk, D. Imre, Aerosol Sci. Technol. 39 (2005) 554.
[2] V.J. Murray, J. Mass Spectrom. 35 (2000) 585.
[3] N. Erdmann, A. Dell'Acqua, P. Cavalli, C. Gruening, N. Omenetto, J.-P. Putaud, F. Raes, R. Dingenen, Aerosol Sci. Technol. 39 (2005) 377.
[4] R. Mahadevan, D. Lee, H. Sakurai, M.R. Zachariah, J. Phys. Chem. A 106 (2002) 11083.
[5] W.D. Reents, Z. Ge, Aerosol Sci. Technol. 33 (2000) 122.
[6] A.N. Christopher, K.A. Prather, Mass Spectrom. Rev. 19 (2000) 248.
[7] P.G. Carson, K.R. Neubauer, M.V. Johnston, A.S. Wexler, J. Aerosol Sci. 26 (1995) 535.
[8] P.J. McKeown, M.V. Johnston, D.M. Murphy, Anal. Chem. 63 (1991) 2069.
[9] K. Park, D. Lee, A. Rai, D. Mukherjee, M.R. Zachariah, J. Phys. Chem. B 109 (2005) 7290.
[10] K.R. Neubauer, M.V. Johnston, A.S. Wexler, Int. J. Mass Spectrom. Ion Process. 151 (1995) 77.
[11] P.T.A. Reilly, A.C. Lazar, R.A. Gieray, W.B. Whitten, J.M. Ramsey, Aerosol Sci. Technol. 33 (2000) 135.
[12] Z. Ge, A.S. Wexler, M.V. Johnston, J. Colloid Interface Sci. 183 (1996) 68.
[13] D.B. Kane, M.V. Johnston, Environ. Sci. Technol. 34 (2000) 4887.
[14] Z. Ge, A.S. Wexler, M.V. Johnston, Environ. Sci. Technol. 32 (1998) 3218.
[15] J. Cabalo, A. Zelenyuk, T. Baer, R.E. Miller, Aerosol Sci. Technol. 33 (2000) 3.
[16] B.D. Morrical, D.P. Fergenson, K.A. Prather, J. Am. Soc. Mass Spectrom. 9 (1998) 1068.
[17] E. Woods, G.D. Smith, R.E. Miller, T. Baer, Anal. Chem. 74 (2002) 1642.
[18] S. Wang, C.A. Zordan, M.V. Johnston, Anal. Chem. 78 (2006) 1750.
[19] D. Lee, K. Park, M.R. Zachariah, Aerosol Sci. Technol. 39 (2005) 162.
[20] S.H. Kim, B.Y.H. Liu, M.R. Zachariah, Chem. Mater. 14 (2002) 2889.
[21] J.H. Kim, V.I. Babushok, T.A. Germer, G.W. Mulholland, S.H. Ehrman, J. Mater. Res. 18 (2003) 1614.
[22] R.L. Armstrong, Appl. Opt. 23 (1984) 148.
[23] A.A. Lushnikov, A.E. Negin, J. Aerosol Sci. 24 (1993) 707.
[24] H.M. Milchberg, S.J. McNaught, E. Parra, Phys. Rev. E: Stat., Nonlinear, Soft Matter Phys. 64 (2001) 056402/1.
[25] L.P.K. Zhou, H.M. Milchberg, M.R. Zachariah, Aerosol Sci. Technol., 2006, submitted for publication.
[26] E. Parra, I. Alexeev, J. Fan, K.Y. Kim, S.J. McNaught, H.M. Milchberg, J. Opt. Soc. Am. B: Opt. Phys. 20 (2003) 118.
[27] K. Park, A. Rai, M.R. Zachariah, J. NanoParticle Res. 8 (2006) 455.